AGU PUBLICATIONS

Geophysical Research Letters

RESEARCH LETTER
10.1002/2015GL063201

Key Points:
- SIF contains information on both APAR and LUE
- SIF per APAR correlates with LUE and is higher during cloudy days
- Satellite-based fluorescence measurements agree with tower-based measurements

Supporting Information:
- Figures S1–S9

Correspondence to:
J. Tang,
jtang@mbl.edu

Citation:
Yang, X., J. Tang, J. F. Mustard, J.-E. Lee, M. Rossini, J. Joiner, J. W. Munger, A. Kornfeld, and A. D. Richardson (2015), Solar-induced chlorophyll fluorescence that correlates with canopy photosynthesis on diurnal and seasonal scales in a temperate deciduous forest, *Geophys. Res. Lett.*, *42*, 2977–2987, doi:10.1002/2015GL063201.

Received 21 JAN 2015
Accepted 20 MAR 2015
Accepted article online 24 MAR 2015
Published online 19 APR 2015

Solar-induced chlorophyll fluorescence that correlates with canopy photosynthesis on diurnal and seasonal scales in a temperate deciduous forest

Xi Yang[1,2], Jianwu Tang[1,2], John F. Mustard[1], Jung-Eun Lee[1], Micol Rossini[3], Joanna Joiner[4], J. William Munger[5], Ari Kornfeld[6], and Andrew D. Richardson[7]

[1]Department of Earth, Environment and Planetary Sciences, Brown University, Providence, Rhode Island, USA, [2]The Ecosystems Center, Marine Biological Laboratory, Woods Hole, Massachusetts, USA, [3]Remote Sensing of Environmental Dynamics Laboratory, DISAT, Universit`a degli Studi Milano-Bicocca, Milan, Italy, [4]NASA Goddard Space Flight Center, Greenbelt, Maryland, USA, [5]School of Engineering and Applied Sciences and Department of Earth and Planetary Sciences, Harvard University, Cambridge, Massachusetts, USA, [6]Department of Global Ecology, Carnegie Institution for Science, Stanford, California, USA, [7]Department of Organismic and Evolutionary Biology, Harvard University, Cambridge, Massachusetts, USA

Abstract Previous studies have suggested that solar-induced chlorophyll fluorescence (SIF) is correlated with Gross Primary Production (GPP). However, it remains unclear to what extent this relationship is due to absorbed photosynthetically active radiation (APAR) and/or light use efficiency (LUE). Here we present the first time series of near-surface measurement of canopy-scale SIF at 760 nm in temperate deciduous forests. SIF correlated with GPP estimated with eddy covariance at diurnal and seasonal scales ($r^2 = 0.82$ and 0.73, respectively), as well as with APAR diurnally and seasonally ($r^2 = 0.90$ and 0.80, respectively). SIF/APAR is significantly positively correlated with LUE and is higher during cloudy days than sunny days. Weekly tower-based SIF agreed with SIF from the Global Ozone Monitoring Experiment-2 ($r^2 = 0.82$). Our results provide ground-based evidence that SIF is directly related to both APAR and LUE and thus GPP, and confirm that satellite SIF can be used as a proxy for GPP.

1. Introduction

Plant photosynthesis, which supports most life on Earth [*Demmig-Adams and Adams*, 2000], is also the largest CO_2 flux in the global carbon cycle [*Ciais et al.*, 2013]. Spatially and temporally explicit estimation of photosynthesis on the ecosystem scale (Gross Primary Production, GPP) can provide important information about when, where, and how much carbon dioxide is absorbed as part of the terrestrial carbon budget [*Parazoo et al.*, 2014; *Zhang et al.*, 2014]. However, direct measurements of GPP are challenging because the net ecosystem exchange (NEE) measured by state-of-the-art methods such as eddy covariance is the combination of both GPP (CO_2 uptake) and ecosystem respiration (CO_2 release). Disentangling these two fluxes involves assumptions that might not hold in certain circumstances [*Reichstein et al.*, 2005]. Currently, three methods are used for the estimation of global GPP: (1) machine learning methods using data from a network of eddy covariance towers, remote sensing, and gridded climatic products [e.g., *Beer et al.*, 2010; *Jung et al.*, 2011]; (2) combination of satellite measurements of vegetation greenness and climate variables through a modeling approach [e.g., *Zhao et al.*, 2005; *Ryu et al.*, 2011; *Field et al.*, 1995]; and (3) process-based models integrated in the Earth system models [e.g., *Lawrence et al.*, 2011; *Schaefer et al.*, 2012]. Multiple sources of uncertainty from model parameterization and explanatory variables can be propagated during the estimation of global GPP [*Beer et al.*, 2010], calling for other independent estimates.

Chlorophyll pigments absorb photons that power photosynthesis. Some of the photons are reemitted at a longer wavelength, in a process called chlorophyll fluorescence. This phenomenon provides a way to estimate photosynthesis using fluorescence. Most previous chlorophyll fluorescence research was conducted using the Pulse Amplitude Modulation (PAM) method in the lab and field [*Baker*, 2008; *Genty et al.*, 1989; *Richardson and Berlyn*, 2002; *van der Tol et al.*, 2014]. Alternatively, high spectral resolution spectrometers have been used to measure steady state fluorescence, for example, the solar-induced chlorophyll fluorescence (SIF) that is emitted during absorption of sunlight by chlorophyll. More recently, the instruments to measure SIF from orbiting platforms (e.g., from the Japanese Greenhouse gases Observing SATellite, GOSAT; or Global Ozone Monitoring Experiment-2, GOME-2) provide a means for estimating GPP from space-based SIF

retrievals [e.g., *Frankenberg et al.*, 2011; *Guanter et al.*, 2012; *Joiner et al.*, 2011, 2013]. The spatial and temporal patterns of satellite-derived SIF are highly correlated with those of GPP derived using state-of-the-art methods, although it has been shown that SIF-GPP relationship is biome specific [*Guanter et al.*, 2012]. There have been some field studies to measure SIF [*Meroni et al.*, 2009; *Rossini et al.*, 2010, 2012; *Perez-Priego et al.*, 2005; *Daumard et al.*, 2012; *Zarco-Tejada et al.*, 2013; *Guanter et al.*, 2013]. However, continuous measurements of SIF along with CO_2 flux measurements using the eddy covariance method are rare [*Balzarolo et al.*, 2011; *Cheng et al.*, 2013; *Damm et al.*, 2010]. Furthermore, most studies have been conducted over croplands or shrublands [*Rascher et al.*, 2009; *Zarco-Tejada et al.*, 2012], yet SIF measurements in deciduous forests have not been reported.

An additional question arises as to whether SIF at 760 nm properly represents GPP or if they merely correlate to a common "hidden" variable. GPP can be thought of as the product of the absorbed photosynthetically active radiation (APAR) times the plant's light use efficiency (LUE), i.e., the conversion rate of photons to CO_2 uptake:

$$\mathrm{GPP} = \mathrm{APAR} \times \mathrm{LUE} \tag{1}$$

SIF can be formulated in a similar way [*Guanter et al.*, 2014]:

$$\mathrm{SIF} = \mathrm{APAR} \times \mathrm{SIF}_{\mathrm{yield}} \tag{2}$$

where $\mathrm{SIF}_{\mathrm{yield}}$ is the emitted SIF per photon absorbed. Since fluorescence is most directly a response to absorbed radiation, one may ask whether the SIF-GPP relationship only reflects the relationship between SIF and APAR, or whether SIF also contains information on LUE, and thus more closely represents GPP. Continuous measurements of canopy SIF under different light conditions and plant phenological stages could help answer this question [*Frankenberg et al.*, 2011; *Porcar-Castell et al.*, 2014].

In this study, we developed a novel spectroscopic system and obtained the first high-frequency time series of canopy SIF in temperate deciduous forests. We estimated GPP using data from a nearby eddy covariance tower. With these measurements, we aim to address the following questions: (1) how does SIF change seasonally and how is it controlled by environmental factors in a temperate deciduous forest? (2) Does SIF contain information on APAR and/or LUE? (3) How do the tower-based and satellite-based observations of SIF compare with each other? Answers to those questions can provide ground-based evidence for using SIF as a proxy for GPP at the global scale.

2. Methods

2.1. Harvard Forest Environmental and CO_2 Exchange Measurements

The study site is in Harvard Forest (42.538 N, 72.171 W), which is a mixed temperate forest in central Massachusetts, USA. The dominant deciduous tree species are red oak (*Quercus rubra*) and red maple (*Acer rubrum*), with a few scattered yellow birch (*Betula alleghaniensis*). The forest age is 70–100 years. The long-term annual mean temperature is about 7.5°C, and the annual precipitation is 1200 mm.

Environmental data were continuously collected every half an hour. These data included air temperature and relative humidity (HMP45C, Vaisala, Finland), air pressure (CS105, Vaisala, Finland), incident photosynthetically active radiation above the canopy ($\mathrm{PAR}_{\mathrm{above}}$) and canopy-reflected PAR ($\mathrm{PAR}_{\mathrm{reflect}}$) from two quantum sensors (PQS-1, Kipp & Zonen B.V., Delft, Netherlands), and the average of understory PAR ($\mathrm{PAR}_{\mathrm{under}}$) from three of the same sensors. A sunshine sensor was used to measure diffuse ($\mathrm{PAR}_{\mathrm{diff}}$) and total PAR ($\mathrm{PAR}_{\mathrm{tot}}$) (BF-5, Delta-T Devices, Cambridge, UK). We defined the days when the daily mean diffuse PAR fraction ($\mathrm{PAR}_{\mathrm{diff}}/\mathrm{PAR}_{\mathrm{tot}}$) >50% as cloudy. The absorbed PAR (APAR) every 30 min was calculated according to equation (3). Daily PAR and APAR were calculated as the mean values of observations between 6:00 A.M. and 6:00 P.M. ($\mathrm{PAR}_{\mathrm{mean}}$, $\mathrm{APAR}_{\mathrm{mean}}$).

$$\mathrm{APAR} = \mathrm{PAR}_{\mathrm{above}} - \mathrm{PAR}_{\mathrm{reflect}} - \mathrm{PAR}_{\mathrm{under}} \tag{3}$$

An eddy covariance tower (Harvard Forest Environmental Monitoring Station, EMS) measured CO_2 exchange between the forest and atmosphere [*Urbanski et al.*, 2007]. We used the method in *Reichstein et al.* [2005] to partition daytime NEE into GPP and ecosystem respiration. Daily GPP was calculated as the sum of 30 min GPP of each day (hereafter: $\mathrm{GPP}_{\mathrm{EC}}$). The light use efficiency (LUE) was calculated as $\mathrm{GPP}_{\mathrm{EC}}/\mathrm{APAR}$.

Narrowband silicon photodiode sensors mounted on the top of the tower (~10 m above the canopy) measure incoming (0° viewing zenith angle, field of view—FOV—is 180°) and reflected light (inclined downward at an angle of 30° below horizontal, FOV = 25°) at 860 nm, 655 nm, 570 nm, 530 nm, and 470 nm,

which were used to calculate reflectance at each wavelength (ρ_{860}, ρ_{655}, ρ_{570}, ρ_{530} and ρ_{470}, Skye 1850, Llandrindod Wells, UK). We then calculated the normalized difference vegetation index (NDVI), the enhanced vegetation index (EVI), and the Photochemical Reflectance Index (PRI) as follows [*Huete et al.*, 2002; *Gamon et al.*, 1992]:

$$\mathrm{NDVI} = \frac{\rho_{860} - \rho_{655}}{\rho_{860} + \rho_{655}} \tag{4}$$

$$\mathrm{EVI} = 2.5\frac{\rho_{860} - \rho_{655}}{\rho_{860} + 6\rho_{655} - 7.5\rho_{470} + 1} \tag{5}$$

$$\mathrm{PRI} = \frac{\rho_{530} - \rho_{570}}{\rho_{530} + \rho_{570}} \tag{6}$$

2.2. Tower-Based Measurements of Solar-Induced Fluorescence

We designed a novel system (FluoSpec) to measure SIF (Figure S1). FluoSpec was deployed in the field from 21 June to 26 October 2013 about 5 m above the canopy on the top of a tower (~1.4 km from the EMS tower). Note that although $\mathrm{GPP_{EC}}$ and SIF were measured at different locations, we assume that eddy covariance tower measurements are representative for a relatively homogeneous landscape in these locations. The key component of FluoSpec is a spectrometer with a spectral resolution of ~0.13 nm (full width at half maximum, FWHM) between 680 nm and 775 nm (HR2000+, OceanOptics, Inc., Dunedin, Florida). The spectrometer was connected to an inline fiber optic shutter (FOS-2x2-TTL, OceanOptics, Inc.) with two ports, each of which was connected to a fiber optic. One of the fiber optics was pointed toward the tree canopy (facing north; FOV: 25°; viewing zenith angle: 30°), while the other one was attached with a cosine corrector (CC-3, OceanOptics, Inc.) pointed toward the sky to collect incident light from 180° FOV [*Zarco-Tejada et al.*, 2013]. The shutter switched between input fibers to collect the signal from either the canopy or sky at one time.

The spectrometer first collected solar irradiance (integrating time: 5 s), then the shutter immediately switched to measure canopy radiance (integrating time: 5 s). Every 5 min the system completed a measurement cycle with one irradiance measurement and the mean of 59 canopy radiance measurements. By measuring solar irradiance and canopy radiance sequentially, we assume that each irradiance measurement provides a "reference" for the subsequent canopy radiance measurement. All measurements were corrected for dark current.

Radiometric and wavelength calibrations were performed prior to and one time during the field campaign using a radiometric calibration light source (LS-1-CAL, OceanOptics, Inc.) and wavelength calibration light source (HG-1, OceanOptics, Inc.). The raw data collected by the spectrometer were then converted to irradiance ($\mathrm{mW/m^2/nm}$) and radiance ($\mathrm{mW/m^2/sr/nm}$) [*Perez-Priego et al.*, 2005].

We used the spectral fitting methods to extract the SIF by exploiting the oxygen absorption (O_2-A) band at 760 nm [*Meroni et al.*, 2009] (for details, see supplementary information). We discarded data when the fitting algorithm $R^2 < 0.99$. Half-hourly SIF ($\mathrm{SIF_{30min}}$) was produced by averaging all SIF measurements of good quality during each time period. We calculated daily mean SIF ($\mathrm{SIF_{mean}}$, mean SIF between 6 am and 6 pm) to represent the emission of SIF of each day. Daily $\mathrm{SIF_{yield}}$ was calculated as the average of half-hourly $\mathrm{SIF_{yield}}$:

$$\mathrm{SIF_{yield}} = \left(\sum \mathrm{SIF_{30\,min}}/\mathrm{APAR_{30\,min}}\right)/N \tag{7}$$

where $\mathrm{APAR_{30\ min}}$ is the half-hourly mean APAR (umol photon/$\mathrm{m^2/s}$) and N is the number of half-hourly measurements. To compare with weekly satellite data, we also calculated the weekly average of sunny day SIF using SIF at 09:30 am (satellite local passing time) measured on days with diffuse PAR fraction < 0.5 (see section 2.3).

Using irradiance and radiance spectra, we calculated canopy reflectance between 680 nm and 775 nm. Similar to equation (4), we calculated NDVI and a normalized difference index (NDI, or Chl NDI as in *Richardson et al.* [2002]) for each sampling interval as in equation (5) [*Garrity et al.*, 2010; *Rossini et al.*, 2010;

Gitelson and Merzlyak, 1994]. NDI is designed for the detection of canopy chlorophyll content. Daily NDVI and NDI, defined as follows, are averaged values between 6:00 A.M. and 6:00 P.M. NDVI in equation (8) is defined slightly different from the one in equation (4) because of the wavelength limit of the spectrometer.

$$\mathrm{NDVI} = \frac{\rho_{750} - \rho_{685}}{\rho_{750} + \rho_{685}} \tag{8}$$

$$\mathrm{NDI} = \frac{\rho_{750} - \rho_{705}}{\rho_{750} + \rho_{705}} \tag{9}$$

2.3. Satellite Measurements of Solar-Induced Fluorescence

We compared tower-based SIF with satellite-based SIF from GOME-2 (the Global Ozone Monitoring Experiment-2), which is an UV/visible spectrometer that measures top-of-atmosphere radiance between 240 and 790 nm. Radiance data that cover 734–758 nm (resolution: ~0.5 nm FWHM) were used to estimate SIF with the method of *Joiner et al.* [2013]. We used the gridded data set of GOME-2 SIF (level 3, version: v25) with spatial resolution of 0.5° latitude × 0.5° longitude. SIF was extracted from a 3 × 3 window (1.5° × 1.5°s) centered on Harvard Forest between June and October in 2013. Since GOME-2 SIF was extracted for 740 nm, we multiplied GOME-2 SIF with 0.582 using the method suggested in *Joiner et al.* [2013] to approximate SIF at 760 nm using Soil Canopy Observation Photochemistry and Energy fluxes (SCOPE) model [*van der Tol et al.*, 2009] (see supporting information).

2.4. Estimating GPP Using MODIS Algorithm

Based on the Moderate Resolution Imaging Spectroradiometer (MODIS) GPP algorithm, we estimated daily GPP ($\mathrm{GPP_{MOD}}$) as a reference to compare with the SIF-GPP relationship [*Running et al.*, 2004].

$$\mathrm{GPP} = 0.45\varepsilon_{\max} F_{\mathrm{SW}} f_{\mathrm{APAR}} S_{\mathrm{VPD}} S_T \tag{10}$$

where $\varepsilon_{\max} = 0.001044$ ($\mathrm{kg\,C\,MJ^{-1}}$), which is the maximum light use efficiency for temperate deciduous forest. F_{SW} is the measured shortwave radiation. f_{APAR} was calculated as $\mathrm{APAR/PAR_{above}}$. S_{VPD} and S_T are scale factors for VPD (Vapor Pressure Deficit) and temperature (see *Running et al.* [2004] for details). All of these parameters are from meteorological station in Harvard Forest.

In addition, the MODIS 8 day 1 km GPP product (MOD17A2, hereafter $\mathrm{GPP_{SAT}}$) for the Harvard Forest pixel was extracted to compare with GPP estimated from the EMS eddy covariance data. We used the quality control flag in the MODIS GPP product to exclude bad data points (only data with quality control flag equal to 0 or 32 were included).

3. Results

Tower-based $\mathrm{SIF_{mean}}$ gradually declined from 0.8 to 1.0 $\mathrm{mW/m^2/sr/nm}$ during the summer to ~0.2 $\mathrm{mW/m^2/sr/nm}$ by the end of the growing season. Similarly, daily $\mathrm{GPP_{EC}}$ decreased from ~12 $\mathrm{g\,C/m^2/day}$ to 1 $\mathrm{g\,C/m^2/day}$ (Figure 1a). Both SIF and $\mathrm{GPP_{EC}}$ showed large day-to-day variations, which was mainly driven by the variations in $\mathrm{PAR_{mean}}$ and, therefore, $\mathrm{APAR_{mean}}$ ($R^2 = 0.684$ and 0.671, respectively; Figures 1b, S2b, S3a, and S3d). Daily mean VPD and air temperature only explained a small portion of the seasonal variations in $\mathrm{SIF_{mean}}$ and $\mathrm{GPP_{EC}}$ (for SIF, $R^2 = 0.352$ and 0.346; for GPP, $R^2 = 0.115$ and 0.306; see Figure S3).

The seasonal pattern (June to October 2013) of $\mathrm{SIF_{mean}}$ agrees well with that of daily $\mathrm{GPP_{EC}}$ ($R^2 = 0.725$; Figures 1a and 2a), which is consistent with the findings using satellite SIF [*Frankenberg et al.*, 2011]. Since satellites like GOSAT, GOME-2, and OCO-2 measure SIF during a specific time of day (local passing time, ~13:30 for GOSAT and OCO-2, and 09:30 for GOME-2), we also compared tower-based SIF we measured at these times with daily $\mathrm{GPP_{EC}}$, as satellite-based SIF was often compared with daily integrated GPP in previous works [*Frankenberg et al.*, 2011; *Joiner et al.*, 2014]. SIF at both local times are significantly correlated with daily $\mathrm{GPP_{EC}}$ (Figure S4a) and $\mathrm{GPP_{EC}}$ at both local times (Figure S4b). The correlation between daily GPP estimated using the MODIS algorithm ($\mathrm{GPP_{MOD}}$, with local meteorological data as inputs) and $\mathrm{GPP_{EC}}$ is slightly weaker ($R^2 = 0.612$; Figure S5d). Similarly, the MODIS 8 day GPP product ($\mathrm{GPP_{SAT}}$) explained ~50% of the variance in $\mathrm{GPP_{EC}}$ but underestimated $\mathrm{GPP_{EC}}$ in the summer ($R^2 = 0.502$;

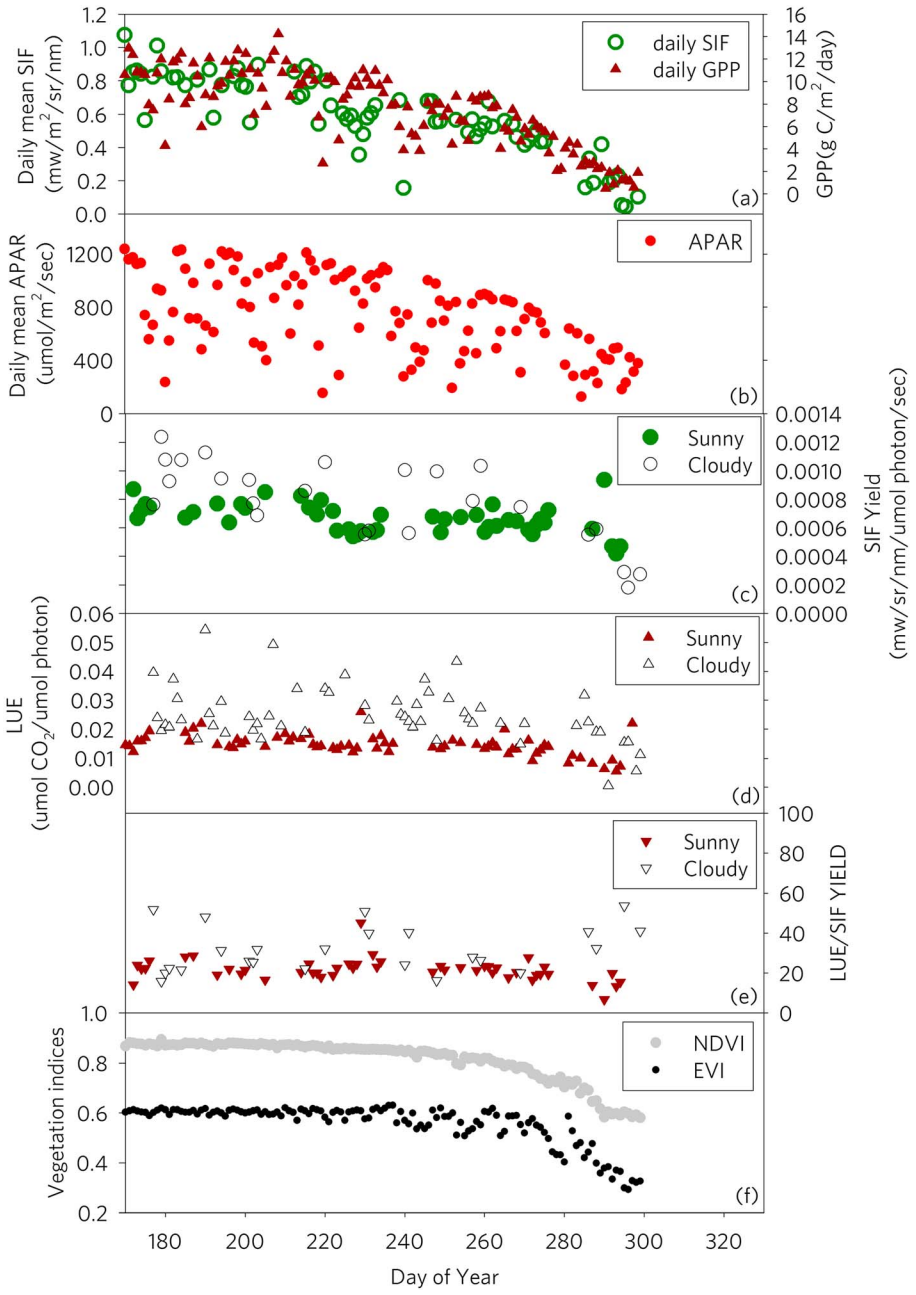

Figure 1. Seasonal patterns of (a) daily mean solar-induced fluorescence (SIF) compared with Gross Primary Productivity (GPP) estimated from eddy covariance tower measurements, (b) daily Absorbed Photosynthetic Active Radiation (APAR), and (c) SIF yield (SIF/APAR). Green dots are from sunny days (diffuse/total radiation < 50%), and black circles are from cloudy days (diffuse/total radiation > 50%), (d) midday light use efficiency (LUE), (e) the ratio between LUE and SIF yield, and (f) NDVI and EVI from narrowband silicon photodiode sensors.

Figure S5a). We found a significant correlation between SIF_{mean} and APAR ($R^2 = 0.794$, $p < 0.0001$; Figure 2d), while the vegetation indices (NDVI and EVI) clearly saturated at high GPP and APAR (Figures 2b, 2c, 2e, and 2f). Specifically, when $GPP_{EC} > 8$ g C/m^2/day, NDVI and EVI showed little change, which was the case for most of the days between June and September. Similar results have been found for croplands and grasslands [*Guanter et al.*, 2014]. NDVI and NDI measured with high spectral resolution spectrometers (see section 2.2) showed similar seasonal trajectories as NDVI measured with narrowband photodiode sensors (Figure S6).

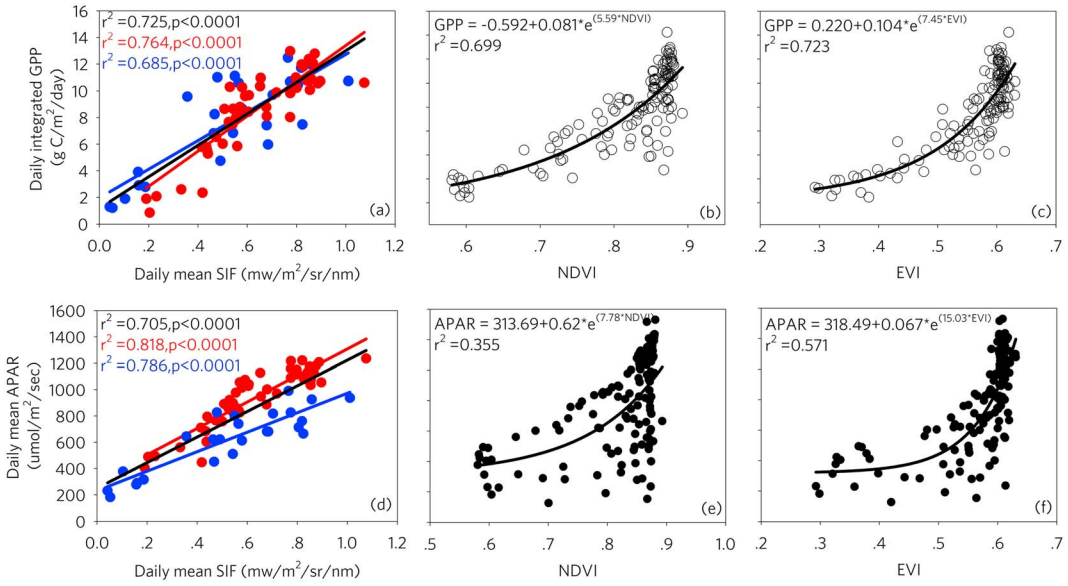

Figure 2. Scatterplots between daily integrated GPP and (a) daily mean SIF, (b) NDVI, and (c) EVI. The scatterplots between daily mean APAR and (d) daily mean SIF, (e) NDVI, and (f) EVI. In Figure 2a, red dots are from sunny days, red line is the linear regression between sunny day GPP and SIF: GPP = 13.21*SIF + 0.19 ($r^2 = 0.764$, $p < 0.0001$); blue dots are from cloudy days, and blue line is the linear regression between cloudy day GPP and SIF: GPP = 10.76*SIF + 1.97 ($r^2 = 0.685$, $p < 0.0001$). For all the days (black line), GPP = 11.82*SIF + 1.19 ($r^2 = 0.725$, $p < 0.0001$). In Figure 2d, red dots are from sunny days, red line is the linear regression between sunny day APAR and SIF: APAR = 1004.73* SIF + 303.64 ($r^2 = 0.818$, $p < 0.0001$); blue dots are from cloudy days, and blue line is the linear regression between cloudy day APAR and SIF: APAR = 741.59* SIF + 231.43 ($r^2 = 0.786$, $p < 0.0001$). For all the days (black line), APAR = 970.36* SIF + 250.29 ($r^2 = 0.705$, $p < 0.0001$). For the relationship between NDVI and GPP (black line in Figure 2b): GPP = −0.592 + 0.081*exp(5.59*NDVI) ($R^2 = 0.699$); EVI and GPP (black line in Figure 2c): GPP = 0.220 + 0.104*exp(7.451*EVI) ($R^2 = 0.723$); NDVI and APAR (black line in Figure 2e): APAR = 313.568 + 0.623*exp(7.881*NDVI) ($R^2 = 0.355$); EVI and APAR (black line in Figure 2f): APAR = 318.485 + 0.067*exp(15.03*EVI) ($R^2 = 0.571$).

To remove the influence of APAR (equations (2) and (3)), we analyzed the relationship between SIF_{yield} (SIF/APAR) and LUE (GPP/APAR). SIF_{yield} is generally 1 order of magnitude smaller than LUE (since usually less than 2% of the absorbed photon is reemitted as fluorescence), but SIF_{yield} shows significantly positive correlation with LUE ($r^2 = 0.39$, $p < 0.0001$; Figure 3). Moreover, as PRI is often used as a proxy for LUE [*Gamon et al.*, 1992; *Hall et al.*, 2008], we compared SIF_{yield} and PRI, which similarly showed a statistically significant relationship ($r^2 = 0.31$, $p < 0.0001$; Figure 3). SIF_{yield} and LUE increased with diffuse light fraction (PAR_{diff}/PAR_{tot}) (Figures 1c, 1d, and S7). Both SIF_{yield} and LUE generally showed higher values during the cloudy days compared with sunny days, consistent with expected increases in efficiency of both fluorescence and photosynthesis under diffuse light (Figure S8) [*Gu et al.*, 2003].

Diurnal SIF measurements (30 min interval) averaged for each month showed a typical hump shape with a steady increase in the morning and decline in the afternoon (Figure 4). The diurnal patterns of SIF were similar to those of GPP ($r^2 = 0.80$). The magnitude of both GPP and SIF declined as the season progressed into fall (Figures 4a and 4e).

Weekly mean sunny day SIF at 09:30 A.M. measured on the ground agreed with GOME-2 SIF converted to approximate SIF at 760 nm ($R^2 = 0.82$; Figure 5; for conversion details, see supporting information), with mean values of GOME-2 SIF are generally higher than those measured on the ground. Overall, the mean value of GOME-2 SIF showed a decreasing trend from the midsummer, consistent with our ground-based estimation of SIF.

4. Discussion

Here we presented the first continuously measured SIF over diurnal and seasonal time scales in temperate deciduous forests. Most importantly, we have used this data set to assess whether SIF is merely a proxy for

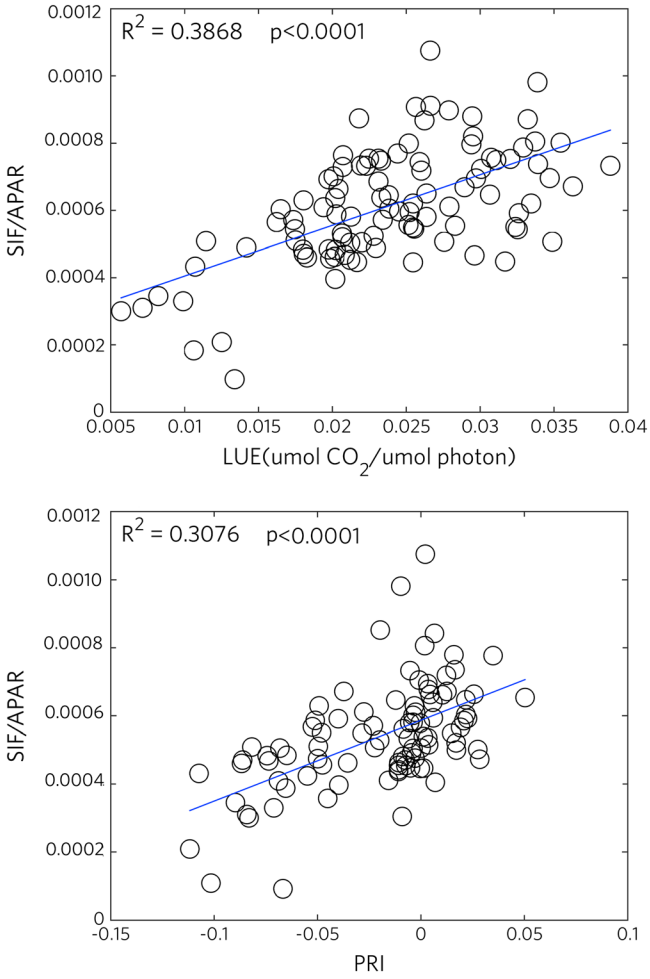

Figure 3. Relationships between (top) SIF_{yield} and LUE and (bottom) SIF_{yield} and PRI. Blue lines in both plots are linear regression between two variables.

APAR, or SIF contains more information that makes it particularly relevant to GPP (i.e., APAR × LUE). Our results suggest that SIF contains information about *both* APAR and LUE.

SIF generally decreases from midsummer to late fall. Superimposed on this pattern is a pronounced day-to-day variation that is highly correlated with PAR (and therefore APAR: in our study we found a nearly 1:1 relationship between the two variables for the study period, $R^2 = 0.996$, Figure S9), as well as a strong diurnal pattern (Figure 4). We interpret these results as suggesting that SIF is mainly driven by APAR, since variations in APAR are much larger than the other component in equation (2)—SIF_{yield} (Figures 1b and 1c). The results also suggest that SIF can be considered as a good estimator of APAR, potentially complement the existing APAR products or ground observation methods based on the above and below canopy measurements of PAR [*Frankenberg et al.*, 2012; *Jenkins et al.*, 2007; *Knyazikhin et al.*, 1998].

As LUE changes with vegetation phenology and plants' responses to various environmental factors including cloudiness [e.g., *Jenkins et al.*, 2007], the significant and positive relationship between SIF_{yield} and LUE suggests that SIF_{yield} responds to variations in these factors as well (Figure S8). Previous studies have shown that chloroplastic heat dissipation (nonphotochemical quenching, NPQ) is the main driver of the variations in fluorescence and photosystem yields, and the positive correlation between SIF_{yield} and LUE is consistent with the results from photosynthesis models parameterized using fluorescence measured by PAM [*Van der Tol et al.*, 2014]. We expected that when NPQ is absent or small, SIF_{yield} and LUE could be negatively correlated. As PRI is positively correlated with LUE throughout the season [*Hall et al.*, 2008] (although a few studies suggest that seasonal PRI is also controlled by pigment pool sizes) [*Wong and Gamon*, 2014], a significant and positive relationship between SIF_{yield} and PRI further supported our finding above. The positive correlation between SIF_{yield} and PRI (and SIF_{yield} and LUE) has also been found for cropland systems [*Middleton et al.*, 2009; *Cheng et al.*, 2013]. Further works need to be extended to other biome types, such as tropical forests or arctic tundra [*Lee et al.*, 2013; *Rocha and Shaver*, 2010].

Within the time period of the measurements, the relationship between SIF and GPP is well characterized by a linear function (Figure 2a). This result does not exclude other forms of the function for the SIF-GPP relationship. At the leaf level, previous works using cotton and tobacco leaves suggested that under high irradiance SIF keeps increasing while GPP tends to saturate [*van der Tol et al.*, 2014], while at the canopy scale, both satellite-based and UAV-based works suggest that a linear function can well characterize the SIF-GPP relationship in various biomes and times of day [*Frankenberg et al.*, 2011; *Guanter et al.*, 2012; *Guanter et al.*, 2014; *Zarco-Tejada et al.*, 2013]. More studies are needed to make measurements of SIF and

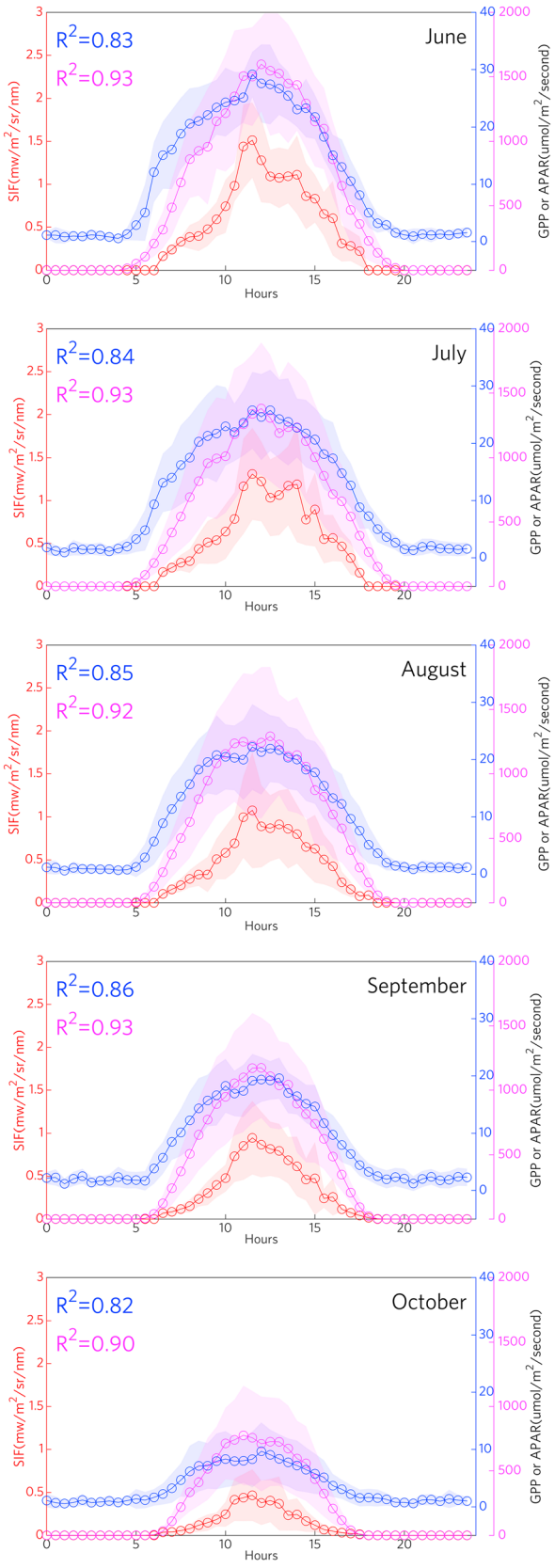

Figure 4. Monthly mean diurnal patterns of SIF, GPP, and APAR. Dots are mean values and shaded areas indicate standard deviations. The *r*-square values for SIF-GPP (blue) and SIF-APAR (magenta) were shown on the top left corners of each subplot.

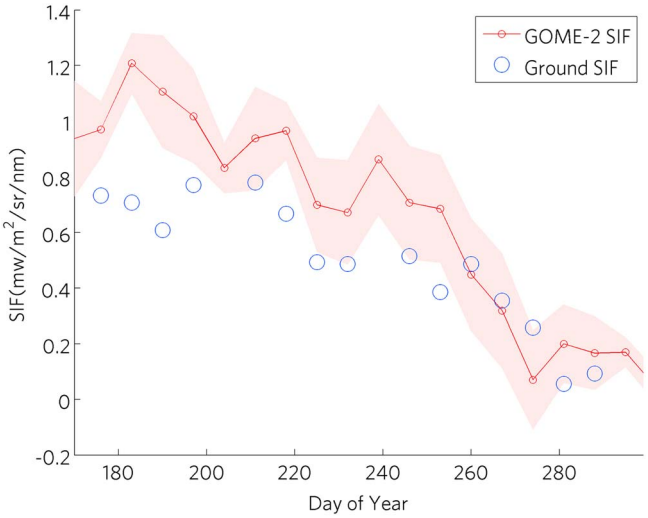

Figure 5. Comparison between ground-measured SIF and GOME-2-derived SIF. Weekly mean GOME-2 SIF in 2013 in the 3 × 3 window centered on Harvard Forest was plotted as red dots (and standard deviation as shaded areas). GOME-2 SIF calculated for 740 nm was converted to 760 nm by multiplying 0.582 (see supporting information). Weekly average of sunny day ground SIF at 09:30 A.M. was plotted as blue circles.

GPP at different environmental conditions (various light, water availability, and CO_2 level) to assess to what extent this linear relationship between SIF and GPP holds.

Chlorophyll fluorescence spectra have two peaks: one in red (~690 nm) and the other in far red (740 nm). Red peak is mainly contributed by Photosystem II activity, while far-red peak is the combination of both Photosystem I and II (PSI and PSII). It has been suggested that PSII fluorescence is related to photochemical processes, thus giving information on LUE [*Porcar-Castell et al.*, 2014; *Rossini et al.*, 2015]. In our study, we estimated SIF at 760 nm, which is thus the combination of both PSI and PSII fluorescence at 760 nm. Measurements of both red and far-red fluorescence can provide a more complete picture of canopy photosynthesis.

The diurnal patterns of SIF we observed may be controlled by both physiological and optical (directionality) factors. When solar zenith angle varies throughout the day, the proportion of sunlit and shaded leaves the FluoSpec "sees" varies [*Damm et al.*, 2015]. As sunlit and shaded leaves receive different amount of PAR, SIF emitted from these two groups of leaves differs. Disentangling the physiological and directionality controls on SIF using coupled radiative transfer and leaf biochemistry model is the next step [*Van der Tol et al.*, 2009; *Van der Tol et al.*, 2014; *Hilker et al.*, 2008]. Additionally, moving (or broken) cloud cover might dramatically change the irradiance spectra within a short period of time (even within 5 min), and the depth of O_2A band can be significantly affected, while the Fraunhofer line might be less affected [*Frankenberg et al.*, 2011]. Future research is needed to test Fraunhofer lines approaches.

Here we show for the first time that satellite observations of SIF agree well with ground-based retrievals. Although tower- and satellite-based measurements of SIF represent different spatial scales (satellite 0.5° × 0.5° per pixel versus tower ~3 m × 3 m), we found a strong linear temporal correlation between tower and satellite retrievals with only slightly higher absolute values for satellite-based SIF estimation ($R^2 = 0.82$). One possible reason for the difference between the magnitude of tower-based and satellite-based SIF is that we assumed a fixed shape of fluorescence emission spectrum when converting GOME-2 SIF at 740 nm to 760 nm. However, the shape of the fluorescence spectrum could change when chlorophyll content changes [*Buschmann*, 2007]. The differences between tower and satellite measurements in terms of defining cloudy days can also partly explain the difference between the two types of measurements of SIF: although both excluded cloudy days, the GOME-2 level 3 gridded data exclude data with effective cloud fractions (which is the approximation of the amount of surface not seen by the satellite) > 0.3, while our tower observations exclude $PAR_{diff}/PAR_{tot} > 0.5$. Vegetation indices such as NDVI, EVI, and narrowband NDI that are commonly used as indicators of canopy greenness showed a clear saturation effect when compared with GPP and APAR (Figures 2 and S6). These results provide support for the future use of satellite SIF products to assess photosynthetic activity [*Guanter et al.*, 2014; *Joiner et al.*, 2014]. We note that a multiscale comparison between tower-, airborne-based, and satellite measurements (e.g., currently Orbiting Carbon Observatory-2, OCO-2 [*Frankenberg et al.*, 2014], future Flourescence Explorer mission [*Rascher et al.*, 2009], and Tropospheric Monitoring Instrument, [*Veefkind et al.*, 2012]) satellite measurements should be carried out to fully validate satellite SIF retrievals and explore the potential of SIF for GPP estimation.

With this unique data set of continuous measurements of SIF, we show that SIF is significantly correlated with GPP estimated from the eddy covariance method. Furthermore, SIF appears to be more than just a proxy for

APAR: the same amount of APAR produced more SIF (SIF_{yield}) under cloudy days comparing to sunny days and SIF_{yield} is significantly correlated with LUE, thus demonstrating that SIF incorporates information about both APAR and LUE (the two components of GPP). Our results demonstrate that SIF measurements contain information about ecosystem functioning and thus could be considered as standard measurements along with CO_2 exchange measurements in carbon flux monitoring networks such as AmeriFlux [*Baldocchi et al.*, 2001] and the National Ecological Observatory Network [*Keller et al.*, 2008].

Acknowledgments

We thank the Editor and three anonymous reviewers for the constructive comments. We thank Joe Berry for insightful suggestions on several versions of the manuscript, Christiaan van der Tol for sharing the SCOPE code, Pablo Zarco-Tejada for the help with the design of FluoSpec, Mark Vanscoy from Harvard Forest and Jerome Girard from MBL with the installation of FluoSpec, and Marc Mayes, Shalanda Grier, Will Werner, and Zhunqiao Liu for the help with fieldwork. We thank Harvard Forest Long-Term Ecological Research site to provide the space and help with the fieldwork, and the weather data used in this study. This research was supported by Marine Biological Laboratory start-up funding for J.T. and the Brown University-Marine Biological Laboratory graduate program in Biological and Environmental Sciences. J.T. was partially supported by the U.S. Department of Energy Office of Biological and Environmental Research grant DE-SC0006951 and the National Science Foundation grants DBI-959333 and AGS-1005663. A.D.R. acknowledges support from the National Science Foundation's Macrosystems Biology (award EF-1065029) and LTER (award DEB-1237491) programs. Meteorological data are downloaded from Harvard Forest LTER (http://harvardforest.fas.harvard.edu/). For the use of solar-induced fluorescence data, please contact Xi Yang (geoxiyang@gmail.com) or Jianwu Tang (jtang@mbl.edu).

The Editor thanks two anonymous reviewers for their assistance in evaluating this paper.

References

Baker, N. R. (2008), Chlorophyll fluorescence: A probe of photosynthesis in vivo, *Annu. Rev. Plant Biol.*, *59*(1), 89–113.

Baldocchi, D., et al. (2001), FLUXNET: A new tool to study the temporal and spatial variability of ecosystem-scale carbon dioxide, water vapor, and energy flux densities, *Bull. Am. Meteorol. Soc.*, *82*(11), 2415–2434.

Balzarolo, M., et al. (2011), Ground-based optical measurements at European flux sites: A review of methods, instruments and current controversies, *Sensors*, *11*, 7954–7981.

Beer, C., et al. (2010), Terrestrial gross carbon dioxide uptake: Global distribution and covariation with climate, *Science*, *329*(5993), 834–838.

Buschmann, C. (2007), Variability and application of the chlorophyll fluorescence emission ratio red/far-red of leaves, *Photosynth. Res.*, *92*(2), 261–271.

Cheng, Y.-B., E. Middleton, Q. Zhang, K. Huemmrich, P. Campbell, L. Corp, B. Cook, W. Kustas, and C. Daughtry (2013), Integrating solar induced fluorescence and the photochemical reflectance index for estimating gross primary production in a cornfield, *Remote Sens.*, *5*(12), 6857–6879, doi:10.3390/rs5126857.

Ciais, P., et al. (2013), Carbon and Other Biogeochemical Cycles, in *Climate Change 2013: The Physical Science Basis. Contribution of Working Group I to the Fifth Assessment Report of the Intergovernmental Panel on Climate Change*, edited by T. F. Stocker et al., Cambridge Univ. Press, Cambridge, U. K., and New York.

Damm, A., et al. (2010), Remote sensing of Sun-induced fluorescence to improve modeling of diurnal courses of gross primary production (GPP), *Global Change Biol.*, *16*(1), 171–186.

Damm, A., L. Guanter, W. Verhoef, D. Schläpfer, S. Garbari, and M. Schaepman (2015), Impact of varying irradiance on vegetation indices and chlorophyll fluorescence derived from spectroscopy data, *Remote Sens. Environ.*, *156*, 202–215, doi:10.1016/j.rse.2014.09.031.

Daumard, F., Y. Goulas, S. Champagne, A. Fournier, A. Ounis, A. Olioso, and I. Moya (2012), Continuous monitoring of canopy level Sun-induced chlorophyll fluorescence during the growth of a *Sorghum* field, *IEEE Trans. Geosci. Remote Sens.*, *50*, doi:10.1109/TGRS.2012.2193131.

Demmig-Adams, B., and W. W. Adams (2000), Photosynthesis: Harvesting sunlight safely, *Nature*, *403*(6768), 371–374.

Field, C. B., J. T. Randerson, and C. M. Malmström (1995), Global net primary production: Combining ecology and remote sensing, *Remote Sens. Environ.*, *51*(1), 74–88.

Frankenberg, C., J. B. Fisher, J. Worden, G. Badgley, S. S. Saatchi, J.-E. Lee, G. C. Toon, A. Butz, M. Jung, and A. Kuze (2011), New global observations of the terrestrial carbon cycle from GOSAT: Patterns of plant fluorescence with gross primary productivity, *Geophys. Res. Lett.*, *38*, L17706, doi:10.1029/2011GL048738.

Frankenberg, C., C. O'Dell, L. Guanter, and J. McDuffie (2012), Remote sensing of near-infrared chlorophyll fluorescence from space in scattering atmospheres: Implications for its retrieval and interferences with atmospheric CO_2 retrievals, *Atmos. Meas. Tech.*, *5*(8), 2081–2094.

Frankenberg, C., C. O'Dell, J. Berry, L. Guanter, J. Joiner, P. Köhler, R. Pollock, and T. E. Taylor (2014), Prospects for chlorophyll fluorescence remote sensing from the Orbiting Carbon Observatory-2, *Remote Sens. Environ.*, *147*, 1–12.

Gamon, J. A., J. Penuelas, and C. B. Field (1992), A narrow-waveband spectral index that tracks diurnal changes in photosynthetic efficiency, *Remote Sens. Environ.*, *41*(1), 35–44.

Garrity, S., L. Vierling, and K. Bickford (2010), A simple filtered photodiode instrument for continuous measurement of narrowband NDVI and PRI over vegetated canopies, *Agric. For. Meteorol.*, *150*(3), 489496, doi:10.1016/j.agrformet.2010.01.004.

Genty, B., J. M. Briantais, and N. R. Baker (1989), The relationship between the quantum yield of photosynthetic electron transport and quenching of chlorophyll fluorescence, *Biochim. Biophys. Acta, Gen. Subj.*, *990*(1), 87–92.

Gitelson, A., and M. N. Merzlyak (1994), Spectral reflectance changes associated with autumn senescence of *Aesculus hippocastanum* L. and *Acer platanoides* L. Leaves. Spectral features and relation to chlorophyll estimation, *J. Plant Physiol.*, *143*(3), 286–292.

Gu, L., D. D. Baldocchi, S. C. Wofsy, J. W. Munger, J. J. Michalsky, S. P. Urbanski, and T. A. Boden (2003), Response of a deciduous forest to the Mount Pinatubo eruption: Enhanced photosynthesis, *Science*, *299*(5615), 2035–2038.

Guanter, L., C. Frankenberg, A. Dudhia, P. Lewis, J. Gómez-Dans, A. Kuze, H. Suto, and R. Grainger (2012), Retrieval and global assessment of terrestrial chlorophyll fluorescence from GOSAT space measurements, *Remote Sens. Environ.*, *121*, doi:10.1016/j.rse.2012.02.006.

Guanter, L., M. Rossini, R. Colombo, M. Meroni, C. Frankenberg, J.-E. Lee, and J. Joiner (2013), Using field spectroscopy to assess the potential of statistical approaches for the retrieval of sun-induced chlorophyll fluorescence from ground and space, *Remote Sens. Environ.*, *133*, doi:10.1016/j.rse.2013.01.017.

Guanter, L., et al. (2014), Global and time-resolved monitoring of crop photosynthesis with chlorophyll fluorescence, *Proc. Natl. Acad. Sci. U.S.A.*, *111*(14), E1327–E1333.

Hall, F. G., T. Hilker, N. C. Coops, A. Lyapustin, K. F. Huemmrich, E. Middleton, H. Margolis, G. Drolet, and T. A. Black (2008), Multi-angle remote sensing of forest light use efficiency by observing PRI variation with canopy shadow fraction, *Remote Sens. Environ.*, *112*, 3201–3211.

Hilker, T., N. Coops, F. Hall, T. Black, M. Wulder, Z. Nesic, and P. Krishnan (2008), Separating physiologically and directionally induced changes in PRI using BRDF models, *Remote Sens. Environ.*, *112*(6), 2777–2788, doi:10.1016/j.rse.2008.01.011.

Huete, A., K. Didan, T. Miura, E. P. Rodriguez, X. Gao, and L. G. Ferreira (2002), Overview of the radiometric and biophysical performance of the MODIS vegetation indices, *Remote Sens. Environ.*, *83*(1–2), 195–213.

Jenkins, J. P., A. D. Richardson, B. H. Braswell, S. V. Ollinger, D. Y. Hollinger, and M. L. Smith (2007), Refining light-use efficiency calculations for a deciduous forest canopy using simultaneous tower-based carbon flux and radiometric measurements, *Agric. For. Meteorol.*, *143*(1–2), 64–79.

Joiner, J., Y. Yoshida, A. P. Vasilkov, Y. Yoshida, L. A. Corp, and E. M. Middleton (2011), First observations of global and seasonal terrestrial chlorophyll fluorescence from space, *Biogeosciences*, *8*(3), 637–651.

Joiner, J., L. Guanter, R. Lindstrot, M. Voigt, A. P. Vasilkov, E. M. Middleton, K. F. Huemmrich, Y. Yoshida, and C. Frankenberg (2013), Global monitoring of terrestrial chlorophyll fluorescence from moderate spectral resolution near-infrared satellite measurements: Methodology, simulations, and application to GOME-2, *Atmos. Meas. Tech.*, *6*, 2803–2823, doi:10.5194/amt-6-2803-2013.

Joiner, J., et al. (2014), The seasonal cycle of satellite chlorophyll fluorescence observations and its relationship to vegetation phenology and ecosystem atmosphere carbon exchange, *Remote Sens. Environ.*, *152*, 375–391.
Jung, M., et al. (2011), Global patterns of land-atmosphere fluxes of carbon dioxide, latent heat, and sensible heat derived from eddy covariance, satellite, and meteorological observations, *J. Geophys. Res.*, *116*, G00J07, doi:10.1029/2010JG001566.
Keller, M., D. Schimel, W. W. Hargrove Jr., and F. M. Hoffman (2008), A continental strategy for the National Ecological Observatory Network (NEON), *Front. Ecol. Environ.*, *6*(5), 282–284.
Knyazikhin, Y., J. V. Martonchik, R. B. Myneni, D. J. Diner, and S. W. Running (1998), Synergistic algorithm for estimating vegetation canopy leaf area index and fraction of absorbed photosynthetically active radiation from MODIS and MISR data, *J. Geophys. Res.*, *103*(D24), 32,257–32,275.
Lawrence, D. M., et al. (2011), Parameterization improvements and functional and structural advances in Version 4 of the Community Land Model, *J. Adv. Model. Earth Syst.*, *3*(3), M03001, doi:10.1029/2011MS000045.
Lee, J. E., et al. (2013), Forest productivity and water stress in Amazonia: Observations from GOSAT chlorophyll fluorescence, *Proc. R. Soc. B*, *280*(1761), 20,130,171.
Meroni, M., M. Rossini, L. Guanter, L. Alonso, U. Rascher, R. Colombo, and J. Moreno (2009), Remote sensing of solar-induced chlorophyll fluorescence: Review of methods and applications, *Remote Sens. Environ.*, *113*(10), 2037–2051.
Middleton, E., Y. Cheng, L. Corp, K. Huemmrich, P. Campbell, Q.-Y. Zhang, W. Kustas, and A. Russ (2009), Diurnal and seasonal dynamics of canopy-level solar-induced chlorophyll fluorescence and spectral reflectance indices in a cornfield, paper presented at Proc. 6th EARSeL SIG Workshop on Imaging Spectroscopy.
Parazoo, N. C., K. Bowman, J. B. Fisher, C. Frankenberg, D. B. Jones, A. Cescatti, O. Pérez-Priego, G. Wohlfahrt, and L. Montagnani (2014), Terrestrial gross primary production inferred from satellite fluorescence and vegetation models, *Global Change Biol.*, *20*(10), 3103–3121, doi:10.1111/gcb.12652.
Perez-Priego, O., P. J. Zarco-Tejada, J. R. Miller, G. Sepulcre-Canto, and E. Fereres (2005), Detection of water stress in orchard trees with a high-resolution spectrometer through chlorophyll fluorescence in-filling of the O_2-A band, *IEEE Trans. Geosci. Remote Sens.*, *43*(12), 2860–2869.
Porcar-Castell, A., E. Tyystjarvi, J. Atherton, C. Tol, J. Flexas, E. Pfundel, J. Moreno, C. Frankenberg, and J. Berry (2014), Linking chlorophyll a fluorescence to photosynthesis for remote sensing applications: Mechanisms and challenges, *J. Exp. Bot.*, doi:10.1093/jxb/eru191.
Rascher, U., et al. (2009), CEFLES2: The remote sensing component to quantify photosynthetic efficiency from the leaf to the region by measuring sun-induced fluorescence in the oxygen absorption bands, *Biogeosciences*, *6*(7), 1181–1198.
Reichstein, M., et al. (2005), On the separation of net ecosystem exchange into assimilation and ecosystem respiration: Review and improved algorithm, *Global Change Biol.*, *11*(9), 1424–1439.
Richardson, A. D., and G. P. Berlyn (2002), Changes in foliar spectral reflectance and chlorophyll fluorescence of four temperate species following branch cutting, *Tree Physiol.*, *22*, 499–506.
Richardson, A. D., S. P. Duigan, and G. P. Berlyn (2002), An evaluation of noninvasive methods to estimate foliar chlorophyll content, *New Phytol.*, *153*(1), 185–194.
Rocha, A. V., and G. R. Shaver (2010), Burn severity influences postfire CO_2 exchange in arctic tundra, *Ecol. Appl.*, *21*(2), 477–489.
Rossini, M., M. Meroni, M. Migliavacca, G. Manca, S. Cogliati, L. Busetto, V. Picchi, A. Cescatti, G. Seufert, and R. Colombo (2010), High resolution field spectroscopy measurements for estimating gross ecosystem production in a rice field, *Agric. For. Meteorol.*, *150*, doi:10.1016/j.agrformet.2010.05.011.
Rossini, M., et al. (2012), Remote sensing-based estimation of gross primary production in a subalpine grassland, *Biogeosciences*, *9*, doi:10.5194/bg-9-2565-2012.
Rossini, M., et al. (2015), Red and far-red sun-induced chlorophyll fluorescence as a measure of plant photosynthesis, *Geophys. Res. Lett.*, doi:10.1002/2014GL062943.
Running, S. W., R. R. Nemani, F. A. Heinsch, M. Zhao, M. Reeves, and H. Hashimoto (2004), A Continuous satellite-derived measure of global terrestrial primary production, *BioScience*, *54*(6), 547–560.
Ryu, Y., et al. (2011), Integration of MODIS land and atmosphere products with a coupled-process model to estimate gross primary productivity and evapotranspiration from 1 km to global scales, *Global Biogeochem. Cycles*, *25*, GB4017, doi:10.1029/2011GB004053.
Schaefer, K., et al. (2012), A model-data comparison of gross primary productivity: Results from the North American Carbon Program site synthesis, *J. Geophys. Res.*, *117*, G03010, doi:10.1029/2012JG001960.
Urbanski, S., C. Barford, S. Wofsy, C. Kucharik, E. Pyle, J. Budney, K. McKain, D. Fitzjarrald, M. Czikowsky, and J. Munger (2007), Factors controlling CO_2 exchange on timescales from hourly to decadal at Harvard Forest, *J. Geophys. Res.*, *112*, G02020, doi:10.1029/2006JG000293.
Van der Tol, C., W. Verhoef, J. Timmermans, A. Verhoef, and Z. Su (2009), An integrated model of soil-canopy spectral radiances, photosynthesis, fluorescence, temperature and energy balance, *Biogeosciences*, *6*(12), 3109–3129.
Van der Tol, C., J. Berry, P. Campbell, and U. Rascher (2014), Models of fluorescence and photosynthesis for interpreting measurements of solar-induced chlorophyll fluorescence, *J. Geophys. Res. Biogeosci.*, *119*, 2312–2327, doi:10.1002/2014JG002713.
Veefkind, J., et al. (2012), TROPOMI on the ESA Sentinel-5 Precursor: A GMES mission for global observations of the atmospheric composition for climate, air quality and ozone layer applications, *Remote Sens. Environ.*, *120*, 7083, doi:10.1016/j.rse.2011.09.027.
Wong, C. Y. S., and J. A. Gamon (2014), Three causes of variation in the photochemical reflectance index (PRI) in evergreen conifers, *New Phytol.*, doi:10.1111/nph.13159.
Zarco-Tejada, P. J., V. González-Dugo, and J. A. J. Berni (2012), Fluorescence, temperature and narrow-band indices acquired from a UAV platform for water stress detection using a micro-hyperspectral imager and a thermal camera, *Remote Sens. Environ.*, *117*, 322–337.
Zarco-Tejada, P. J., A. Morales, L. Testi, and F. J. Villalobos (2013), Spatio-temporal patterns of chlorophyll fluorescence and physiological and structural indices acquired from hyperspectral imagery as compared with carbon fluxes measured with eddy covariance, *Remote Sens. Environ.*, *133*, 102–115.
Zhang, Y., L. Guanter, J. A. Berry, J. Joiner, C. van der Tol, A. Huete, A. Gitelson, M. Voigt, and P. Köhler (2014), Estimation of vegetation photosynthetic capacity from space-based measurements of chlorophyll fluorescence for terrestrial biosphere models, *Global Change Biol.*, doi:10.1111/gcb.12664.
Zhao, M., F. A. Heinsch, R. R. Nemani, and S. W. Running (2005), Improvements of the MODIS terrestrial gross and net primary production global data set, *Remote Sens. Environ.*, *95*(2), 164–176.